# Evaluation of Spinal Anatomy Segmentation Methods using Synthetic Computed Tomography Volumes

Austin Tapp and Michel Audette
Biomedical Engineering Institute,
Computational Modeling and Simulation Engineering
Old Dominion University
Norfolk, VA, USA
e-mail: atapp001@odu.edu

***Abstract*— Severe adolescent idiopathic scoliosis (AIS) is corrected by surgical procedures that necessitate ligament releases. To determine appropriate release allotments, soft tissues must be localized on a patient-specific basis. However, routine computed tomography (CT) imaging precludes traditional, voxel-based soft tissue localization. Fortunately, recent studies have proposed top-down segmentation methods, which elucidate soft tissues using pre-operative CT volumes. While the accuracy of vertebral segmentations obtained from these methods has been determined, the accuracy of soft tissue segmentations has not. To ensure the soft tissue segmentation methods are clinically applicable, soft tissue validation must occur. This study presents an evaluation measure for surmised soft tissues, accomplished through the use of synthetic CT (sCT) volumes. The sCTs have geometrically scoliotic shapes and provide ground truth information, which was used to evaluate soft tissue segmentations and establish their clinical utility. This proposed validation method is achieved fully *in silico* and is generically applicable, allowing future soft tissue elucidation methods to be assessed.**

***Keywords-patient-specific modeling; osseoligamentous mesh; synthetic CT; in silico validation; adolescent idiopathic scoliosis.***

## I. INTRODUCTION

### A. Background

Adolescent idiopathic scoliosis (AIS) affects about 30 million individuals worldwide [1]. If not resolved, AIS can lead to serious back problems, decreased lung capacity, and heart damage. AIS treatments depend on the patient's primary, lateral spine curvature. Severe curvatures, defined by angles greater than 45 degrees, are resolved with invasive surgical interventions like posterior spinal fusion (PSF) [1][2]. PSF surgical outcomes seek to prevent progression, maintain coronal and sagittal alignment, level the shoulders, correct the spinal deformity, and preserve motion segments [1]. Prior to PSF operations, computed tomography (CT) or biplanar X-ray imaging is used to evaluate curvature angles and determine correction strategies [3]. Unfortunately, such images provide little understanding as to how patients will respond intraoperatively during corrective procedures [4]. Thus, extra steps to mobilize the spine are performed, resulting in increased morbidity, operating room time, and patient blood loss [5]. To make operations safer and more efficient, patient-specific, biomechanical, finite element (FE) simulations may be used to explore various corrective strategies and approaches [6]. FE biomechanical simulation offers risk-free ways to determine necessary corrective forces when multi-material, volumetric meshes encompass all patient anatomy, including soft tissues [7]. Unfortunately, the nature of pre-operative CT and X-ray imaging modalities makes it nearly impossible to localize soft tissues and determine required ligament releases needed to mobilize the spine during PSF correction.

### B. Related Work

A recent method for ligament segmentation using a top-down segmentation approach, based on anatomy that is conspicuous in CT imaging, has been proposed [8]. By exploiting an osseoligamentous computer-aided designed (CAD) mesh, context-aware deformable registration of the osseoligamentous mesh onto vertebral anatomy of CT imaging allows for the position of volumetric soft tissues, including ligaments, to be surmised on a patient-specific basis. Fig. 1 shows the method. While registration accuracy of this method has been evaluated for anatomy conspicuous in CT and magnetic resonance imaging (i.e., vertebrae and intervertebral discs, respectively), validation of the ligament positioning has not been performed. Such validation requires that ground truth segmentations of ligaments within CT images be known. However, if ground truth ligament segmentations could be obtained manually, the need for top-down segmentation would be obviated: bottom-up, voxel-based methods would be sufficient to determine ligament positions. The inability to obtain expertly segmented ground truth ligaments presents a serious roadblock. One option for the elucidation of ligament ground truths is through synthetic CT (sCT) imaging. Literature describing synthetic image creation is often focused on the conversion of sCTs from other imaging modalities, namely magnetic resonance imaging (MRI). Methods creating sCTs are wide-ranging and use simple algorithms or computationally expensive, conditional generative adversarial networks [9][10][11]. However, these methods disregard the soft tissues that are conspicuous within MRIs but are non-conspicuous in CTs and do not transfer soft tissues information during MRI to sCT conversion.

 ISBN: 978-1-61208-898-3 

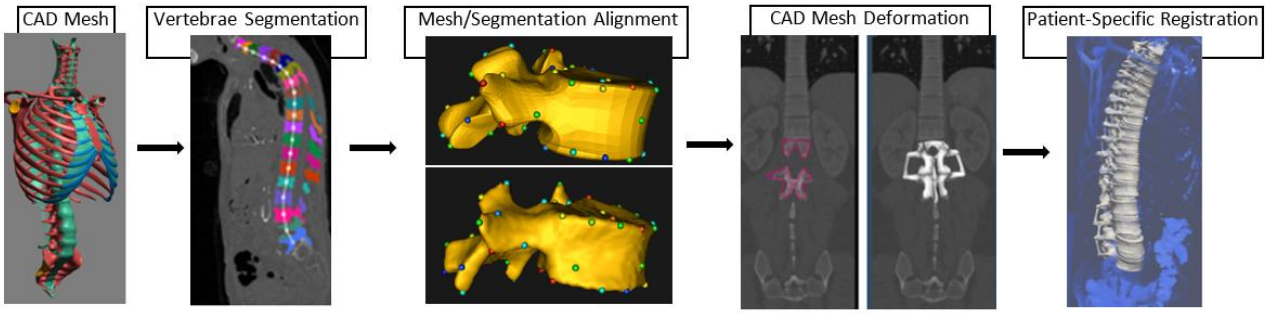


Figure 1. Tapp et al. overview [8]. (Left to right) The method begins with an osseoligamentous CAD torso, with red and green coloring for bones and soft tissues, respectively. Then a patient CT is fed to a neural network, which automatically outputs vertebrae segmentations. CAD vertebrae and vertebrae segments are affinely aligned using a corresponding particles system. This is followed by elastic deformations of the CAD to a patient-specific mesh.

Therefore, an alternative scoliotic sCT volume creation method that maintains soft tissue positioning information is necessary [12]. The method benefits from having its foundation rooted in FE analyses. While many FE studies have explored AIS etiology, they end after scoliotic induction is completed [4][13][14]. If post-study FE meshes containing volumetric or 3-dimensional (3-D) ligaments are converted to sCT volumes, the ligament ground truth segmentation roadblock may be circumvented. AIS-shaped sCT volumes would have corresponding ligament ground truths, provided by the FE meshes. The ligament positions surmised by the top-down segmentation approach could then be validated with the FE mesh-based ground truths. This validation would assist in substantiating methods that localize ligaments in routine CT and X-ray imaging; again, these methods provide a critical step toward determining the minimum number of ligament releases required to mobilize the spine when AIS patients undergo PSF operations.

This study examined the accuracy of all anatomy generated by the top-down segmentation approach using an sCT-based validation measure, which provided 3-D ground truth segmentations for vertebrae, intervertebral discs (IVDs) and other soft tissues. sCT volumes were generated for the lumbar and thoracolumbar sections of the spine with a conversion method that harnesses FE meshes, which contain 3-D bone and soft tissue structures and have been deformed by FE analysis methods to appear geometrically scoliotic. After applying the top-down segmentation method of Tapp et al. to the sCT volumes, the surmised, patient-specific anatomy is compared to its respective ground truths. This contribution provides the medical image analysis community with the means to verify the accuracy of methods surmising soft tissues, which are practically impossible to manually segment.

## II. METHODS

### A. Creating Synthetic CT Volumes

The FE spine mesh with 3-D ligaments was developed into a synthetic CT volume that is geometrically scoliotic with the process seen in Fig. 2. The process begins by running FE analyses on FE spine meshes. All FE spine meshes contain tetrahedral, 4-node elements that represent: cortical bone, trabecular bone, posterior bone, vertebral endplates, cartilaginous endplates, nucleus pulposus, annulus matrices, annulus fibers and any spinal ligaments. Material properties for elements of all the FE spine mesh are derived from published studies and are shown in Table 1 [15][16][17][18]. A neo-Hookean model represents only trabecular and posterior bone, the nucleus pulposus and both endplates. Cortical bone uses an orthotropic elastic material. The annulus fibrosus is represented with a compressible Holmes-Mow matrix model and fiber components that apply an exponential power law to describe strain energy density. All 3-D ligaments use the same viscoelastic, coupled, transversely-isotropic Mooney-Rivlin material, which was experimentally determined [17][18]. This study utilized FEBio for FE analysis because of its credibility and open-source availability [19]. Scoliotic shapes were induced phenomenologically, by applying simplistic boundary conditions to FE spine meshes. Linear, prescribed, transverse displacement was applied to all nodes comprising the bony structure of the most central vertebra. To imitate that FE spine was part of a larger column, upper vertebral endplates of the most superior vertebrae and lower vertebral endplates of the most inferior vertebra were fixed. Linear boundary conditions were continuously applied in a transient manner until a subsequent time step caused deformations that prematurely terminated the run of the FE analysis.

Once the FE spine meshes undergo FE analyses to appear scoliotic, meshes are converted to sCT volumes. First, FE spine meshes are exported as triangular surface meshes, and the surface mesh is resampled into a volume using a true CT. The resampling maintains the mesh's structure but adjust its size and spacing to match that of the true CT. Then, using Elastix, the true CT is deformably registered onto the newly created mesh volume, which is structurally identical to the surface mesh it was created from [20]. This volume-to-volume registration method consistently transfers Hounsfield unit values from the true CT to the sCT. A mask that obscures bone bereft portions of the true CT will explicitly preserve the original image intensity values that surround bony structures of the true CT and rapidly produce sCT volumes with Hounsfield unit (HU) intensity values for all portions of the image. The triangular surface mesh that was exported after the FE analysis is the ground truth for the sCT. The ground truth can be stripped of bone or soft tissues to allow for the use of each type of anatomy, as needed.

 ISBN: 978-1-61208-898-3 

TABLE I. MATERIAL PROPERTY CONSTANTS OF THE FE MESHES

| Structure | Materials | Property Constants | Ref |
|---|---|---|---|
| Cortical bone | Orthotropic elastic | $E_1$ = 8k MPa, $E_2$ = 8k MPa, $E_3$ = 12k MPa, $v_{12}$ = 0.4, $v_{23}$ = 0.3, $v_{31}$ = 0.35 | 15,16 |
| Trabecular bone | Neo-Hookean | E = 100 MPa, v = 0.2 | 15,16 |
| Posterior bone | Neo-Hookean | E = 3500 MPa, v = 0.3 | 15,16 |
| Vertebral endplate | Neo-Hookean | E = 1000 MPa, v = 0.3 | 15,16 |
| Cartilaginous endplate | Neo-Hookean | E = 23.8 MPa, v = 0.42 | 15,16 |
| Nucleus pulposus | Neo-Hookean | E = 1 MPa, v = 0.49 | 15,16 |
| Facet cartilage | Neo-Hookean | E = 30 MPa, v = 0.4 | 15,16 |
| Annulus matrix | Holmes-Mow | E = 1 MPa, $\beta^1$ = 3.4 | 15,16 |
| Annulus fibers | Fiber-exp-power | $\alpha^2$ = 65, $\beta^3$ = 2, $\xi^4$ = 0.296 MPa | 15,16 |
| **3-D Ligaments** | Coupled transversely-isotropic Mooney-Rivlin | $c_1$ = 2.1660 MPa, $c_3$ = 0.2677 MPa, $c_4$ = 83.0594, $c_5$ = 535.5720, $k^5$ = 436.845 MPa, $\lambda^6$= 1.0498 | 17,18 |

a. For 3-D ligaments: 1: exponential stiffening coefficient, 2: coefficient of exponential argument, 3: power of exponential argument, 4: fiber modulus, 5: bulk modulus, 6: max fiber straightening stretch

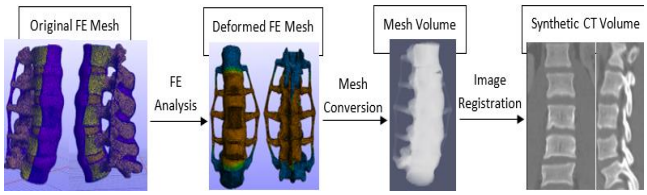


Figure 2. Overview of the FE mesh to sCT volume method [12]. The FE mesh is deformed, converted to an image registered with a true CT volume.

## B. Generating Volume-Specific, Osseoligamentous Meshes

While more details can be found in the manuscript by Tapp et al., a brief outline of how to develop a volume-specific osseligamentous spine mesh is described below. As mentioned, because of the inconspicuous presentation of soft tissues in CT imaging, segmenting ligaments by intrinsic voxel-based or neural network (NN) techniques is precluded. Therefore, the top-down, segmentation approach must begin with an anatomist-developed CAD mesh of a torso. The torso's structure is characteristic of a healthy, average, adult human and contains bone, ligament, and some other soft tissues, but no muscle. The deformable registration process of the CAD mesh first requires it to be approximately positioned within the CT image space. To accomplish this, vertebral segmentations, attained from the sCT using a deep learning NN, are utilized as a basis for the positioning of the CAD mesh vertebrae. The deep learning NN obtains vertebral segmentations in a fully automatic, 3-step, coarse-to-fine process [21]. The first step predicts approximate x and y coordinates of the spine as $\hat{x}_{spine} \in \mathbb{R}^2$ using a U-Net variant. The second step localizes the center of the vertebral bodies through a Spatial-Configuration-Net (SC-Net), which is comprised of 2 components that work together to determine local landmark appearance while considering the landmark's spatial configuration. The predicted spine coordinate $\hat{x}_{spine}$ of the first step is used to narrow the portions of the sCT processed. Finally, individual vertebrae are segmented with the same U-Net variant as in Step 1. The centroids output by SC-Net provide a semantic label that crops the region around the landmark, allowing vertebrae to be segmented at full resolution and independently of one another. The resulting output segmentations are resampled to their original input position in the overall sCT volume. The CAD meshes are then aligned to relevant sCT image space by an affine transformation that exploits these NN-derived vertebrae segmentations. The CAD vertebrae meshes and the NN vertebrae segmentations are populated with surface particles that spatially correspond between both vertebrae's surfaces [22]. The particles guide an initial affine transform.

After the affine transform of the CAD mesh onto relevant sCT space, the CAD mesh is deformably registered [23]. This occurs by lumping all CAD mesh vertices as a single mass component, which is driven toward pertinent CT voxels. The meshes' vertex motions are solved using an implicit Euler scheme that determines Newtonian dynamics-based forces described by $f_i = \alpha_i(R_i - P_i)$, where $P_i$ is a vertex position and $f_i$ is the force that attracts $P_i$ towards its target vertex, $R_i$. Weighting factors consider image gradients and upper-quartile voxel intensities to encourage CAD vertebrae deformation toward highly conspicuous aspects of the sCT, i.e., the sCT's vertebrae. Simultaneously, anatomy around the vertebral portions of the CAD mesh is locally deformed due to the vertices mass grouping, surmising positions of soft tissues, such as ligaments, that are inconspicuous in the sCT.

## C. Validation Metrics

Several validation metrics were employed to evaluate the volume-specific meshes generated through the deformable registration of the osseoligamentous CAD mesh onto sCT volumes. The metrics compare the post-registered meshes with their respective ground truth segmentations, which are given during the FE spine mesh to sCT conversion pipeline. The volume-specific meshes are converted to segmentations prior to comparison to their ground truths. For more detailed descriptions of the comparisons utilized, we refer the reader to Yeghiazaryan & Voiculescu [24]. Briefly, three accuracy metrics for segmentation that are commonly considered to be gold standards are described. The first metric, Dice similarity coefficient (DSC), volumetrically compares the number of segment elements that overlap with the total elements found in the ground truth segmentations; the DSC of a segment compared to itself would be 1. A second metric, average Hausdorff distance (aHD), compares the overall surfaces of segmentations, measuring disparity, in millimeters (mm), between the surface a segmentation and the corresponding surface of its ground truth. The third metric is Intersection over Union (IoU), also known as Jaccard similarity. This metric is quite similar to DSC, but penalizes false positives to a greater degree. Again, a segment compared to itself is equal to 1. Additional metrics that are not described in detail are: 95$^{th}$ percentile HD (95%) in mm, sensitivity (SE), specificity (SP), false positive rate (FP) and false negative rate (FN).

 ISBN: 978-1-61208-898-3 

## III. RESULTS

### A. Synthetic CT Volumes

The CAD-based FE meshes with 3-D ligaments were deformed using prescribed displacement to create a scoliotic curve profile. For the CAD-based lumbar mesh, the L3 vertebra was displaced by 5.1 mm and for the CAD-based thoracolumbar mesh, the T10 vertebra was displaced 6.5 mm. The two CAD-based meshes were then successfully converted into two sCT images using true CT volumes from their respective anatomical regions. The lumbar sCT volume is seen in Fig. 2 and the thoracolumbar sCT volume is shown next to its true CT in Fig. 3. Both sCT volumes had voxel intensity values that remained consistent with their true CT counterparts. sCT voxel values ranged from -1272 to 1716 HUs. Fig. 4 shows histograms that reflect HUs of the lumbar and thoracolumbar sCT volumes and their true CTs.

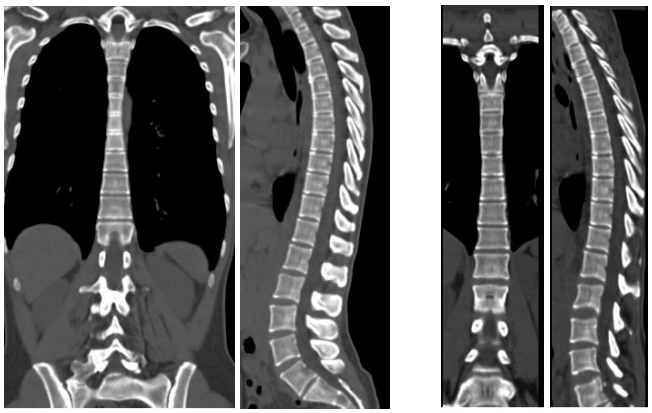

Figure 3. The thoracolumbar sCT (right side) and its true CT (left side).

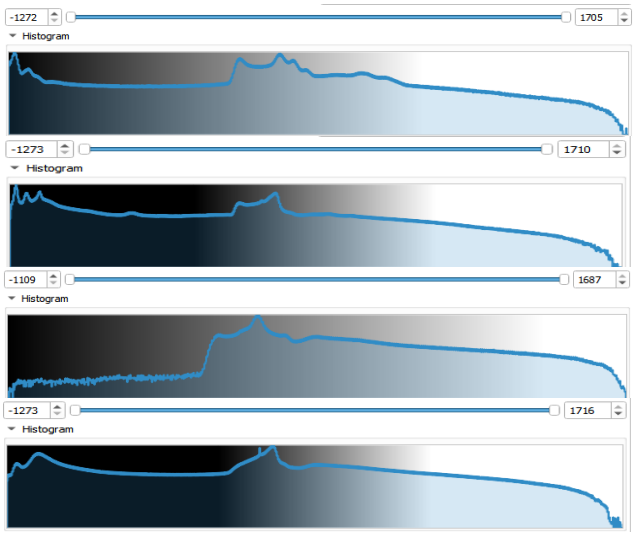


Figure 4. From top to bottom: histograms of the true lumbar CT, lumbar synthetic CT, true thoracolumbar CT and thoracolumbar synthetic CT.

### B. Validating Volume-Specific, Osseoliagmentous Meshes

NN training was done with CT data of MICCAI's VerSe grand challenge (verse2020.grand-challenge.org/). Training and testing was performed with Tensor-flow using a mini-batch size of 1 for all networks, 10,000 iterations for the spine localization network, 50,000 iterations for the vertebrae localization network and 50,000 iterations for the segmentation network. The Adam optimizer with a $10^{-4}$ learning rate was used for Modified U-Nets; the Nesterov optimizer at a $10^{-8}$ learning rate was used for SC-Net [21].

Both volume-specific, osseoligamentous meshes were evaluated with the metrics described in section 2C. The osseoligamentous meshes were assessed as a whole, with the soft tissues removed (i.e., only comparing vertebrae), and with the bone removed (i.e., only comparing soft tissues). Further, to provide a frame of reference and determine the necessity of the affine and deformable registration methods, the NN-derived vertebrae segmentations were also evaluated with bone-only ground truths. Table 2 contains a summary of detailed results for each of these four evaluations. Fig. 5 shows a qualitative view of the 3 ground truth segmentations compared to their meshes during lumbar spine evaluation. Briefly, DSC, aHD and IoU of all anatomy evaluation was determined to be 0.72, 2.4mm and 0.55, respectively for the lumbar meshes and 0.68, 2.1mm and 0.52, respectively for the thoracolumbar meshes. For the vertebrae only evaluation, it is important to note the whole vertebrae, not just vertebral bodies of vertebrae, were evaluated. DSC, aHD and IoU of the vertebrae was determined to be 0.66, 2.27mm and 0.50, respectively for the lumbar meshes and 0.64, 1.97mm and 0.48, respectively for the thoracolumbar meshes. For the soft tissue only comparison, all 3-D ligaments and the IVDs were examined. For the soft tissues of the lumbar patient-specific mesh DSC was 0.46, aHD was 4.5mm and IoU was 0.30. For the soft tissues of the thoracolumbar patient-specific mesh, DSC was 0.50, aHD was 2.9mm and IoU was 0.34. Finally, for unassisted, NN-derived vertebrae segmentations in the lumbar mesh DSC was 0.58, aHD was 2.61mm and IoU was 0.41 while in the thoracolumbar mesh DSC was 0.54, aHD was 3.47mm and IoU was 0.37.

TABLE II. QUANTITATIVE RESULTS SUMMARY. L AND T ARE LUMBAR AND THORACOLUMBAR EVALUATIONS, RESPECTIVELY. ST IS SOFT TISSUE, 8 IS VERETBRAE MESHES OBTAINED WITH [8]'S METHOD, 21 IS VERTBRAE MESHES OBTAINED WITH THE NN. 2C DEFINES ABBREVATIONS AND UNITS.

| Mesh | DSC | aHD | IoU | 95% | SP | SE | FP | FN |
|---|---|---|---|---|---|---|---|---|
| L-all | 0.72 | 2.40 | 0.55 | 6.38 | 0.98 | 0.63 | 0.02 | 0.37 |
| L-ST | 0.46 | 4.46 | 0.30 | 12.4 | 0.99 | 0.33 | 0.01 | 0.67 |
| L-8 | 0.66 | 2.27 | 0.50 | 5.74 | 0.97 | 0.60 | 0.03 | 0.40 |
| L-21 | 0.58 | 2.61 | 0.41 | 5.84 | 1 | 0.41 | 0.00 | 0.59 |
| T-all | 0.68 | 2.08 | 0.52 | 5.67 | 0.97 | 0.63 | 0.02 | 0.37 |
| T-ST | 0.50 | 2.90 | 0.34 | 8.02 | 1 | 0.39 | 0.00 | 0.61 |
| T-8 | 0.64 | 1.97 | 0.48 | 5.31 | 0.98 | 0.60 | 0.02 | 0.40 |
| T-21 | 0.54 | 3.47 | 0.37 | 13.2 | 1 | 0.37 | 0.00 | 0.63 |

 ISBN: 978-1-61208-898-3

## IV. DISCUSSION

The presented evaluation demonstrated that the published method achieves a somewhat decent agreement when comparing all anatomical structures – the soft tissues and the vertebrae. The method also reported better overall scores compared to the current MICCAI vertebrae segmentation challenge winning network for vertebrae in the sCT [21]. The network seems to have struggled significantly when segmenting the sCT volumes, possibly due to their synthetic nature, their zoomed cropping around the region of the spine, or their structurally adjusted shape. Regardless, the poor segmentations caused the downstream methods to perform significantly worse than in previously published studies. In particular, Fig. 5 shows the NN's segmentation results for the transverse processes of the vertebrae guided a completely incorrect placement of the transverse ligaments. Typically, the NN performs quite well on patient CT volumes and allows the downstream affine and deformable registration processes to outperform state of the art methods in related studies. Unfortunately, there are no studies that evaluate all spinal soft tissues, so comparison or discussion of these results is extremely limited. However, given DSC and aHD are weakest in soft tissue evaluations, additional work will need to be considered for better soft tissue fitting. Further, as seen in Fig. 5. the subtraction technique performed to obtain soft tissue ground truths may not be ideal. Alternatively, soft tissues should be exported as their own mesh; the present study subtracted the fully included anatomy ground truth by the bone only ground truth to provide soft-tissue ground truth data and may have resulted in the noted underperformance due to additional, inaccurate "ground truth" information. Finally, scoliotic geometry of sCT volumes were minor. sCT with geometry of moderate to severe scoliotic spines should be tested with Tapp et al. and Payer et al.'s methods [8][21].

### A. Conclusion

This study implemented previously published methods to evaluate the spinal anatomy segmentations derived from the MICCAI vertebral segmentation challenge winning NN and from an emerging top-down segmentation approach. The top-down approach surmises the position of ligaments and soft tissues by exploiting bone structures, like vertebrae, that are conspicuous in CT imaging. By using a sCT that provides 3-D soft tissue ground truths, all portions of patient-specific osseoligamentous meshes developed with the top-down approach can be evaluated. The presented technique quantitatively evaluates the soft tissue positions obtained by the top-down segmentation approach completely *in silico.* This validation technique is required for advancing scoliosis interventions, like PSF, which currently necessitate unknown numbers of ligament releases. Ligaments must first be accurately localized on a patient-specific basis to develop a full patient-specific model that will help to determine ideal ligament release strategies. Corrective procedures like PSF, can be made safer and more efficient by yielding models that contain 3-D ligaments and calculate the number of ligament releases required to mobilize the spine during surgical interventions. Aside from its capability to verify soft tissues in the spinal column, the presented method is broadly applicable for validating the presence of other soft tissues and may be especially beneficial for future studies performed on areas of the knee, shoulder, hand, and foot.

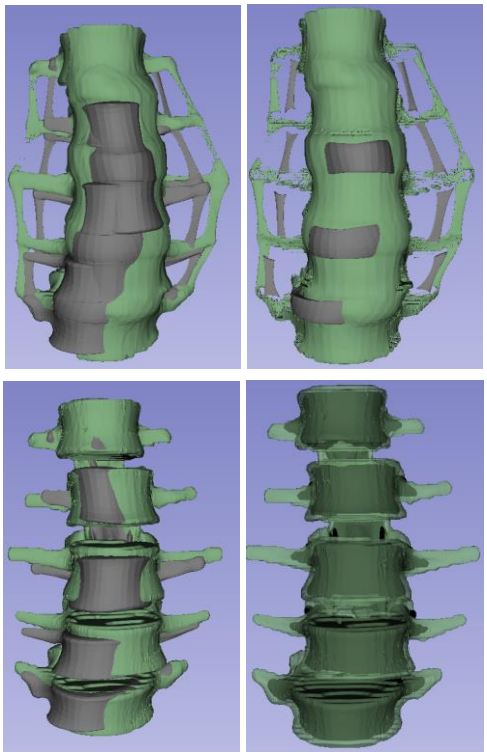

Figure 5. Lumbar Qualitative results. Ground truth is green, meshes evaluated are gray. (top left) All anatomy evaluated, including bone and soft tissue. Then, (top right) soft tissues evaulated; vertebrae are removed. Finally, (bottom left) vertebrae only evaluation using the method of [8] compared to [21]'s segmentations (bottom right).

### B. Future Work

Parameters of the top-down segmentation methodology need to be updated to provide better soft-tissue alignment. The FE meshes must also undergo varied analyses to see what kinds of severe scoliotic curve geometries can be induced. FE meshes with more than one curve are also being considered for development. This breadth of FE meshes, which will be used to produce sCT volumes, may be utilized for additional methodological validation. sCT volumes should encompass an entire spinal column, from the skull to the sacrum for future validation work. Further, the sCT volumes and their ground truths will ultimately be used to train a deep learning neural network that performs one-shot segmentations given the sCT image and the ground truth. The segmentations may include all anatomy or exclusively output soft tissues.

 ISBN: 978-1-61208-898-3 

## REFERENCES


[1] M. Mohamed, J. Trivedi, N. Davidson, and S. Munigangaiah, "Adolescent idiopathic scoliosis: a review of current concepts," Orthopaedic and Trauma, vol. 34, pp. 338-345, Dec. 2020, doi:10.1016/j.mporth.2020.09.003.

[2] Z. B. Cheung, S. Selverian, B.H. Cho, C. J. Ball, S. Kang-Wook and Cho, S, "Idiopathic Scoliosis in Children and Adolescents: Emerging Techniques in Surgical Treatment," World Neurosurgery, vol. 130, pp. e737-742, Oct. 2019, doi:10.1016/j.wneu.2019.06.207.

[3] T. Illés and S. Somoskeöy, "The EOS™ imaging system and its uses in daily orthopaedic practice," International Orthopaedics, vol. 36, pp. 1325-1331, Feb. 2012, doi:10.1007%2Fs00264-012-1512-y.

[4] J. P. Little and C. Adam, "Patient-specific computational biomechanics for simulating adolescent scoliosis surgery: Predicted vs clinical correction for a preliminary series of six patients," International Journal for numerical Methods in Biomedical Engineering, vol. 27, pp. 347-356. Mar. 2011, doi:10.1002/cnm.1422.

[5] L. G. Lenke, et al., "Adolescent idiopathic scoliosis. A new classification to determine extent of spinal arthrodesis," The Journal of Bone & Joint Surgery, vol. 83, pp. 1169-1181, Aug. 2001, doi:10.2106/00004623-200108000-00006.

[6] L. La Barbera, A.N. Larson, J. Rawlinson, and C. E. Aubin, "*In silico* patient-specific optimization of correction strategies for thoracic adolescent idiopathic scoliosis," Clinical Biomechanics, vol. 81, pp. unlisted Jan. 2021, doi:10.1016/j.clinbiomech.2020.105200.

[7] M. Audette, J. Schmid, C. Goodmurphy, M. Polanco, S. Bawab, et al., "Towards a deformable multi-surface approach to ligamentous spine models for predictive simulation-based scoliosis surgery planning," Computational Methods and Clinical Applications for Spine Imaging, vol. 11397, pp. 90-102, Mar. 2019, doi:10.1007/978-3-030-13736-6_8.

[8] A. Tapp, C. Payer, J. Schmid, M. Polanco, et al., "Generation of patient-specific, ligamentoskeletal, finite element meshes for scoliosis correction planning," LNCS., in press.

[9] N. Chegeni, M. Birgani, F. Birgani, D. Fatehi, G. Akbarizadeh, and M. Tahmasbi, "Introduction of a simple algorithm to create synthetic-Computed tomography of the head from magnetic resonance imaging," Journal of Medical Signals and Sensors, vol. 9, pp. 123-129, Apr. 2019, doi:10.4103/jmss.JMSS_26_18.

[10] A. Baydoun, et al., "Dixon-based thorax synthetic CT generation using Generative Adversarial Network," vol. 3-4, pp. unlisted, Dec 2020, doi: 10.1016/j.ibmed.2020.100010.

[11] J. Mangalagiri, "Toward Generating Synthetic CT Volumes using a 3D-Conditional Generative Adversarial Network," ArXivorg, Jan 2021 , https://par.nsf.gov/biblio/10232074.

[12] A. Tapp, M. Polanco, I. Kumi, S. Bawab, et al., "Generating scoliotic computed tomography volumes from finite element spine models," LNCS., in press.

[13] L. Shi, et al., "Biomechanical analysis and modeling of different vertebral growth patterns in adolescent idiopathic scoliosis and healthy subjects," Scoliosis, vol. 6, pp. unlisted, May 2011, doi:10.1186/1748-7161-6-11.

[14] J.F. Sarwark, R. M. Castelein, A. Maqsood, C. E. Aubin, "The Biomechanics of Induction in Adolescent Idiopathic Scoliosis: Theoretical Factors," Journal of Bone and Joint Surgery, vol. 101, pp. e22, Mar 2019, doi:10.2106/JBJS.18.00846.

[15] S.M. Finley, D.S. Brodke, N.T. Spina, C.A. DeDen, and B.J. Ellis, "FEBio finite element models of the human lumbar spine," Computer Methods in Biomechanics and Biomedical Engineering, vol. 21, pp. 444-452, Jan 2018, doi:10.1080/10255842.2018.1478967.

[16] H. Kim, H. Chun, et al., "A validated finite element analysis of nerve root stress in degenerative lumbar scoliosis," Medical & Biological Engineering & Computing, vol. 47, pp. 599-605, Mar. 2009, doi: 10.1007/s11517-009-0463-y.

[17] M. Hortin, Ligament model fidelity in finite element analysis of the human lumbar spine. [Online]. Available from: scholarsarchive.byu.edu/etd/5254. Accessed 09/09/2021.

[18] E. Peña, B. Calvo, M. A. Martínez, M. Doblaré, "A three-dimensional finite element analysis of the combined behavior of ligaments and menisci in the healthy human knee joint," Journal of Biomechanics, vol. 39, pp.1686-1701, doi:10.1016/j.jbiomech.2005.04.030.

[19] S. A. Maas, B. J. Ellis, G.A. Ateshian, J.A. Weiss, "FEBio: Finite elements for biomechanics," Journal of Biomechanical Engineering, vol. 134, Feb. 2012, doi:10.1115/1.4005694.

[20] S. Klein, M. Staring, K. Murphy, M. A. Viergever, and J. P. W. Pluim, "elastix: A Toolbox for Intensity-Based Medical Image Registration," in IEEE Transactions on Medical Imaging, vol. 29, pp. 196-205, Jan. 2010, doi: 10.1109/TMI.2009.2035616.

[21] C. Payer, D. Štern, H. Bischof, M. Urschler, "Coarse to fine vertebrae localization and segmentation with SpatialConfiguration-Net and U-Net," VISIGRAPP, vol. 5, pp. 124-133, Feb. 2020, doi:10.5220/0008975201240133.

[22] J. Cates, S. Elhabian, R. Whitaker, "ShapeWorks: Particle-Based Shape Correspondence and Visualization Software," Statistical Shape and Deformation Analysis, vol. 1, pp. 257-298, Jan. 2017, doi:10.1016/B978-0-12-810493-4.00012-2.

[23] D. Damopoulos, et al., "Segmentation of the proximal femur in radial MR scans using a random forest classifier and deformable model registration," International Journal of Computer Assisted Radiology and Surgery, vol. 14, pp. 545-561, Jan. 2019, doi:10.1007/s11548-018-1899-z.

[24] V. Yeghiazaryan, I. Voiculescu, "Family of boundary overlap metrics for the evaluation of medical image segmentation," Journal of Medical Imaging, vol. 5, pp. 015006, Feb. 2018, doi:10.1117/1.jmi.5.1.015006.


 ISBN: 978-1-61208-898-3 